Curie point depth, thermal gradient and heat flow along the Ethiopia Rift System and adjacent plateaus using spectral evaluation approach: implications for geothermal resources

Samson Hilemichaeil[1,2]* , Tigistu Haile[2] and Gezahegn Yirgu[2]

*Correspondence:
samayn1221@gmail.com;
samson.hmichaeil@aau.edu.et

[1] Kotabe College of Natural and Computational Sciences, Kotabe Education University, Addis Ababa, Ethiopia
[2] School of Earth Science, Addis Ababa University, P.O. Box 1176, Addis Ababa, Ethiopia

Abstract

The Ethiopia Rift System (ERS) is a section of the East African Rift System within Ethiopia extending from the Afar in the northeast to the Kenya border in the southwest. It is apparent that magmatism and magmatic intrusions influence the crustal shape in the ERS resulting in its thinning and the shallowing of magmatic sources at various locations within it. As a consequence, more than 31 volcanoes hosting hydrothermal structures with a conceivable potential to generate massive quantities of geothermal energy have been identified along the ERS. In this study, we map the Curie Point Depth (CDP) over the ERS based on the analysis of aeromagnetic data extracted from the World Digital Magnetic Anomaly Map. Spectral evaluation method was used to estimate the boundaries (top and bottom) of the magnetized crust. Reduced-to-pole (RTP) aeromagnetic records have been divided into 105 (50% overlap) square blocks of 200×200 km size. The Curie temperature (580 °C) of magnetite was used to determine the thermal gradient and the heat drift in the area. The depths obtained for the bottom of the magnetized crust are assumed to correspond to the Curie Depths, where the magnetic layer loses all its magnetization. The determined values of Curie Point Depth, geothermal gradient and heat flow for the 50% overlapped 105 blocks, respectively, range from 8.85 to 55.85 km, 10.38 to 65.54 °C/km and 25.96 to 163.84 mW/m^2. Lower CPD (< 20 km) in the ERS was obtained between Mille and Gewane (southwest Afar), between Adama (Nazret) and Yerer (NMER) and between Wendo Genet and Koti (SMER) localities. These areas, showing low CPD, exhibit excessive geothermal gradient and high heat flow all of which indicate the presence of significant geothermal potential.

Keywords: Main Ethiopia Rift, Curie point depth, Heat flow, Curie temperature, Reduction-to-pole

Introduction

The East African Rift System (EARS) consists of a series of rift segments extending from the Afar Triple Junction at the Red Sea–Gulf of Aden intersection to the Malawi Rift (Bonini et al. 2005). An on-going section of magmatic rifting along a segment of the Red Sea in the Ethiopian Afar offers a notable possibility to constrain relationships amongst volcanism and crustal growth (Ferguson et al. 2010). This section of the Rift is magmatically segmented (Ebinger and Casey 2001; Kurz et al. 2007), seismically energetic (Keranen et al. 2004) region with uplifted flanks and steep border faults which attract quite a number of geoscientific groups to investigate its lithological shape, energetic flood basalt, continental breakup and a region, where continental rifts develop in to oceanic ridges.

Previous findings display that the central portion of the EARS over Ethiopia; the main Ethiopia Rift (MER), is characterized by the occurrence of major transversal lineaments which have an effect on the rift floor and the plateaus surrounding the rift system (Adhana 2014; Corti et al. 2022). The ERS as a whole covers an area of 380,808 km^2 (Fig. 2). Mainly, the primary NE–SW form of the ERS is diverted to WNW–ESE due to the Yerer-Tullu Wellel and Goba–Bonga volcano-tectonic lineaments, staining the transition into a few of the unique MER sectors. At a smaller scale, those transversal structures were interpreted to reflect the reactivation of inherited Neoproterozoic weaknesses more or less parallel to the geometry of the Gulf of Aden (Fig. 1; Abbate and Sagri 1980; Abebe et al. 1998; Korme et al. 2004; Adhana 2014; Corti et al. 2018; Corti et.al. 2022). The Yerer-Tullu Wellel lineament corresponds to a massive gradient within the thickness of the crust and marks the boundary between the northern and southern slices of the northwestern Ethiopian Plateau (Keranen and Klemperer 2008).
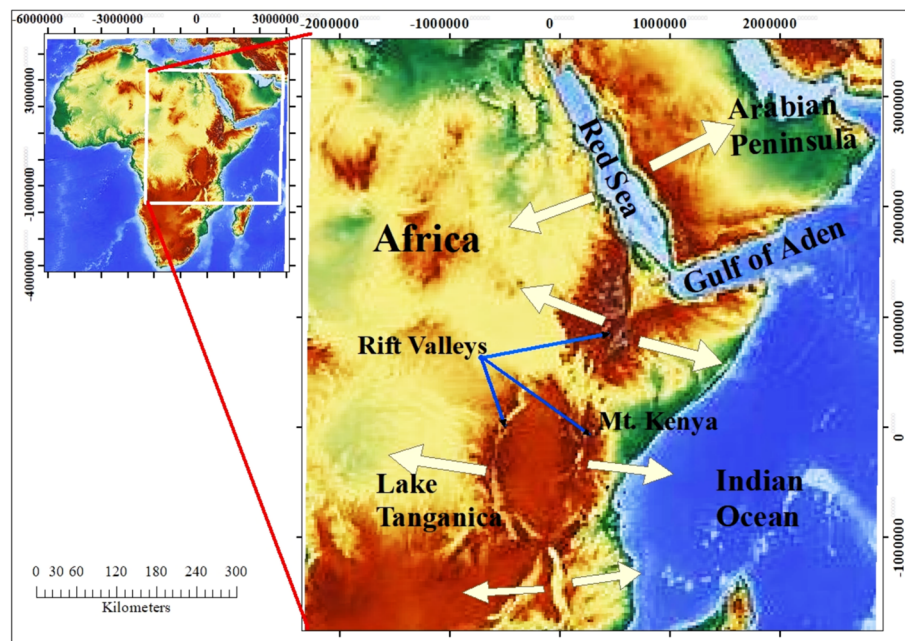

Fig. 1 East African Rift System (EARS) showing the continental extension (break up) between the Nubia–Somalia and the Nubia–Arabia plate boundaries (modified after Saemundsson 2008; Hardarson 2017)
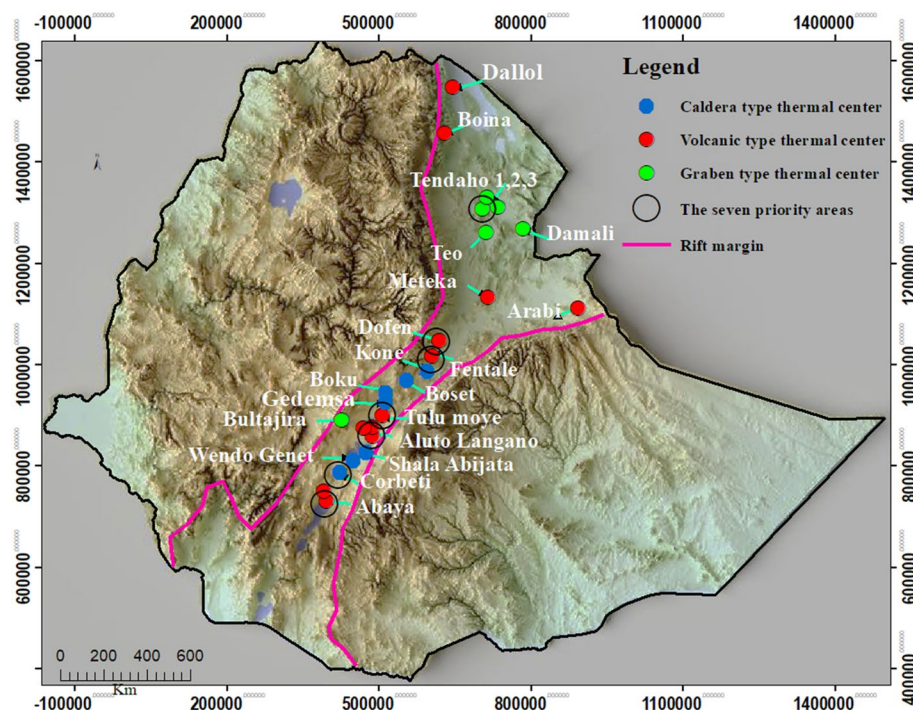
Fig. 2 Map showing the 22 geothermal potential sites in Ethiopia (marked by coloured dots) and the 7 priority areas (marked by black circle; Kebede, 2014, 2021) superimposed on digital elevation model (DEM); the pink bold line indicating the rift margin (Yahya et al. 2022)

The role of magma intrusion and diking as opposed to large offset faults inside the MER is manifested through elongation of the eruptive centres, localization of seismicity and magmatic movement (Casey et al. 2006). There are two end-member eventualities at the formation of these tectono-magmatic segments (TMS). In line with Boccaletti et al. (1999), and segmentation results from change in the direction of extension from NW–SE/orthogonal to E–W/oblique motion of the Nubia–Somalia kinematics (Fig. 1). Alternatively, Ebinger and Casey (2001) suggest that the segments are particularly managed through a manner of the magmatic action in a way similar to oceanic rift processes. It is well apparent that magmatism and magmatic intrusions determine the crustal shape within the MER (Ebinger and Casey 2001; Casey et al. 2006). Geodetic records display that the TMSs are fashioned above or close to the locus of most extension and accommodate 80% of the strain across the rift, indicating that border faults are no longer the locus of extension (Ebinger and Casey 2001; Corti 2009). Comparison with mid-ocean ridges suggests that TMSs mark the sea–continent boundary in rifts with a ready magma supply (Ebinger and Casey 2001; Bastow et al. 2005; Kurtz et al. 2007).

More than 31 volcanoes hosting hydrothermal systems with the capability to generate big quantities of geothermal energy were suggested within the MER (Greenfield et al. 2019). Owing to the presence of a large number of geothermal manifestations all along the Rift, Ethiopia began studies on the geothermal resources of the Rift way back in 1969. Of the 22 prospect areas identified, the government of Ethiopia prioritized 7 fields for the development of the geothermal resource; these are the Corbetti,

Abaya, Tulu Moye, Dofan, Fentale, Aluto-Langano and Tendaho geothermal areas (Fig. 2, Amanu 2018; Kebede 2016).

Geophysical techniques such as seismic survey, magnetotelluric (MT), gravity and magnetics can yield more exact understanding about subsurface structures (faults, dike swarms, magma chambers and intrusions) (Telford et al. 1990). Recent developments in instrumentation, field techniques and powerful interpretation software have increased the use of geophysical investigation for the understanding of geothermal resources and their characteristics. More recent works include the use of satellite-derived magnetic and gravity data to get a synoptic view of potential geothermal areas and their relation with Rift dynamics and associated geologic processes. The main objective of this research is, therefore, to determine Curie Point Depth (CPD), geothermal gradient and heat flow of the ERS and adjacent plateaus using the spectral evaluation method. In this paper, aeromagnetic records that are derived from the World Digital Magnetic Anomaly Map (WDMAM) have been processed, and estimates of CPD, geothermal gradient and heat flow values derived.

Geology

The Ethiopian rift system

The East African Rift System (EARS) is one of the few seismically and volcanically active continental rifts in the world. It extends for about 6,500 km from the Afar Rift in the north to Mozambique in the south. The Ethiopian Rift System (ERS) constitutes the northern sector of this East African Rift System (EARS) and lies between the Northwestern Ethiopia Plateau to the north and west and the South-eastern Ethiopian Plateau to the south (Corti 2013). The ERS extends for more than 1000 km in an NE–SW-to-N–S direction from the Afar depression, at the Red Sea–Gulf of Aden junction (triple junction), passing through central Ethiopia and southwards to the Turkana depression (Fig. 3; Corti 2013). The ERS can be divided into three main sectors: the Afar Rift, the Main Ethiopian Rift (MER) and the South-western Ethiopian Rift. The MER was established as the Nubian and Somalin plates separated during the Miocene period along the East African Rift System (Bonin et al. 2004). The MER is extending in an ESE–WNW direction at a rate of about 2.5 mm/yr (Wolfenden et al. 2004). Within the ERS, the Miocene border faults are thought to be now inactive and extension is focused along the magmatic segments (Ebinger and Casey 2001; Casey et al. 2006; Keir et al. 2006). The rift floor itself is cut by a series of smaller en echelon, right-stepping rift basins of Quaternary to recent age. The Ethiopian flood basalt province which is preserved on the Northwestern and South-eastern Ethiopian plateaus is considered to be the result of a mantle plume magmatism (Courtillot et al. 2003). The flood volcanics consist of approximately 300,000 km^3 of Oligocene–Miocene basalts and associated felsic volcanics that over-lie the uplifted Mesozoic marine sequences (Mickus et al. 2007).

The geology of Afar region

According to Barberi et al. (1975); cited by Abbate et al. (2015), the Afar volcanics can be estimated as a first stage of continental rifting which lasted about 25–20 Ma, and a later stage which initiated 4 Ma during which the oceanic floor in the central portion of Afar began to develop. The most extensive volcanic sequence connected with the second
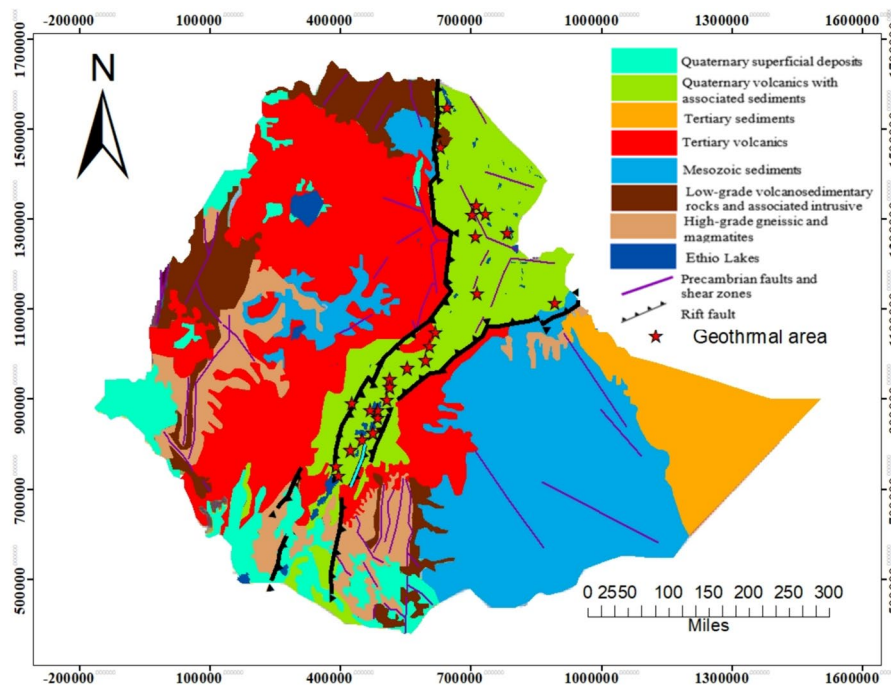
Fig. 3 Geological map of Ethiopia. The area surrounded by black line is the Ethiopian Rift System (modified from Tefera et al. 1996; Abbate et al. 2015)

stage is the Plio-Pleistocene Afar Stratoid Series which covers about two-thirds of the Afar depression. This consists of intermediate basalts, about 1,500 m thick, and lies unconformably on the Dalha Basalts after a phase of magmatic quiescence (Abbate et al. 2015). The northern Afar volcanic range (Erta Ale) parallels the Afar axis with an NNW trend; while to the south the volcanic ranges shift gradually to WNW. A large part of this area consists of fissural eruptions and shield volcanoes with basaltic flows and alkaline to peralkaline silicic rocks. Most of them have been active in historical times, and the Erta Ale volcano exhibits a spectacular lava lake even to date (Fig. 4; Abbate et al. 2015).

Danakil Depression is a Quaternary extension that has thinned the crust to about 16 km, where the rift is below sea level. The Afar Depression is dominated by the Plio-Pleistocene Afar Stratoid Series with only minimal Quaternary magmatism and has an average crustal thickness of about 25 km (Hayward and Ebinger 1996). The East Central Afar region is characterized by a series of major grabens, such as the NW–SE trending Dobi graben. Strain across the Dobi graben is accommodated on high angle normal faults and sinisterly strike-slip faults (Hayward and Ebinger 1996; Beyene 2004). The Southern Afar region is covered by Plio-Pleistocene flood basalts and is cut by narrow NNE–SSW trending Quaternary faults with an average crustal thickness of about 26 km (Fig. 4; Abbate et al. 2015).

The Main Ethiopian Rift (MER)

The Main Ethiopian Rift (MER) which is part of the East African Rift system (EARS), where extensional deformation or rifting began as early as late Oligocene–early Miocene times (Morley et al. 1992; Ghebreab 1998; Ebinger et al. 2000; Bellahsen et al.
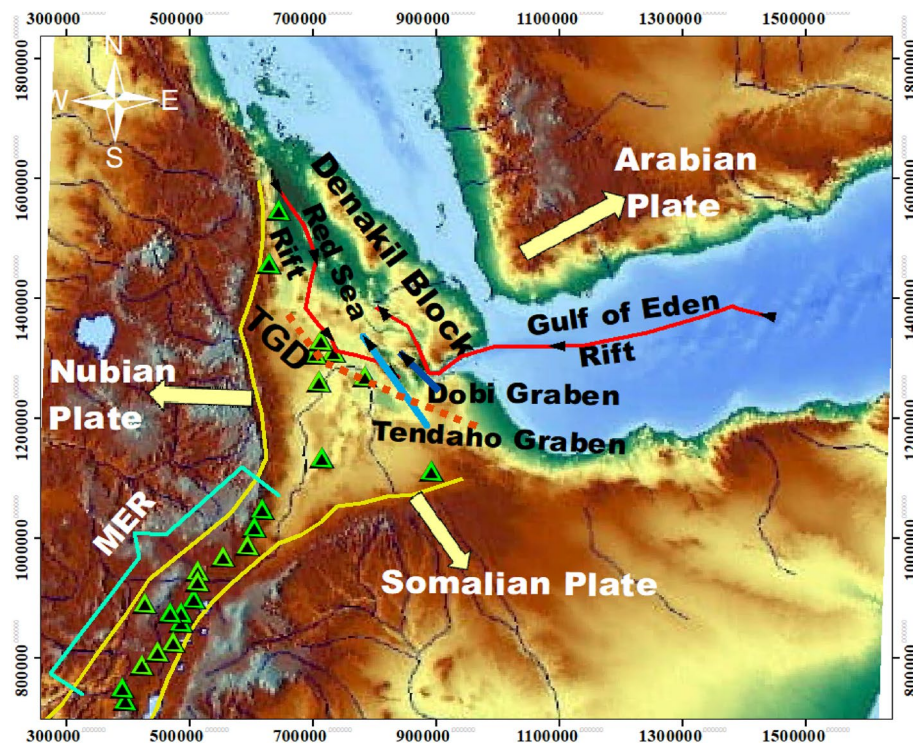
Fig. 4 Geological map of Afar showing fault orientation and direction of rift propagation. Solid yellow lines indicate Miocene border faults, solid red lines denote axes of the Red Sea and Gulf of Aden rifts and beryl green triangle indicate geothermal areas. TGD (Tendaho Gobaad Discontinuity) separating east-central Afar from southwestern Afar (after Reed et al. 2014)

2003). MER is an NNE–SSW-to-N–S trending trough 120 km wide in the Northern Main Ethiopian Rift (NMER), 80 km wide in the Central Main Ethiopian Rift (CMER) and 120 km wide in the Southern Main Ethiopian Rift (SMER), and is 700 km long. Its southern end is bounded by the South-western Ethiopian Rift which itself extends to the Kenya Rift in the Turkana depression. The northern portion of the MER includes discontinuous faults that give rise to major fault escarpments separating the rift depression (Baker et al. 1972). These faults are widely spaced and are characterized by large vertical offsets which are estimated at < 1000 m (Boccaletti et al. 1998). The axis of the MER, known as the Wonji Fault Belt (WFB), started to develop at the beginning of the Quaternary (Meyer et al. 1975), and probably reflects the present-day stress field (Chorowicz et al. 1994; Boccaletti et al. 1998; Ebinger and Casey 2001). Transversal E–W trending structures are found at the Yerer Tullu-Wellel volcano-tectonic lineament (Abebe et al. 1998) and the Goba–Bonga lineament (Abbate and Sagri 1980). This system probably represents inherited structural trends associated with the Gulf of Aden fracture system (Abebe et al. 1998).

Data and methods

Data

Aeromagnetic data used in this research were adopted from the World Digital Magnetic Anomaly Map V2 (WDMAM, http://www.wdmam.org/download.php), permitted by the

International Association of Geomagnetism and Aeronomy (IAGA) in 2015 (Lesur et al. 2016). It was compiled from satellite, marine, aeromagnetic and ground-based magnetic surveys. The data locations were given in WGS84 geodetic system. The Total Magnetic Intensity (TMI) anomaly was derived by subtracting the International Geomagnetic Reference Field (IGRF) values for each station (Fig. 5).

Methods

Reduction to The Pole

Reduction to The Pole (RTP) transformation is a commonly used magnetic data processing method especially for large-scale mapping (Yao 2013). Due to the dipolar nature of the geomagnetic field, magnetic anomalies of the Earth at any inclination and declination out of magnetic pole are asymmetric (Cooper and Cowan 2005; Luo et al. 2010). To tackle this problem, researchers are using the RTP method to process the magnetic data. Pole reduction (RTP) takes the magnetic anomaly as if the body had been laid at the magnetic pole, i.e., the place where the magnetic field is vertical and is magnetized by induction only. Assuming that one has a collection of observed magnetic data gathered on a flat observation surface, if $A_e(u, v)$ is the Fourier transform of the observed magnetic data and $A_P(u, v)$ is the Fourier transform of the vertical magnetic field that would be observed at the same locations where the magnetization is also vertical (the RTP field), then the pole reduction operation in wavenumber domain can be expressed as (Gunn 1975; Luo et al. 2010)

$$Ap(u, v) = \frac{A_e(u, v)}{(sin\mathbf{I} + icos\mathbf{I}sin(D + \theta))^2} \tag{1}$$
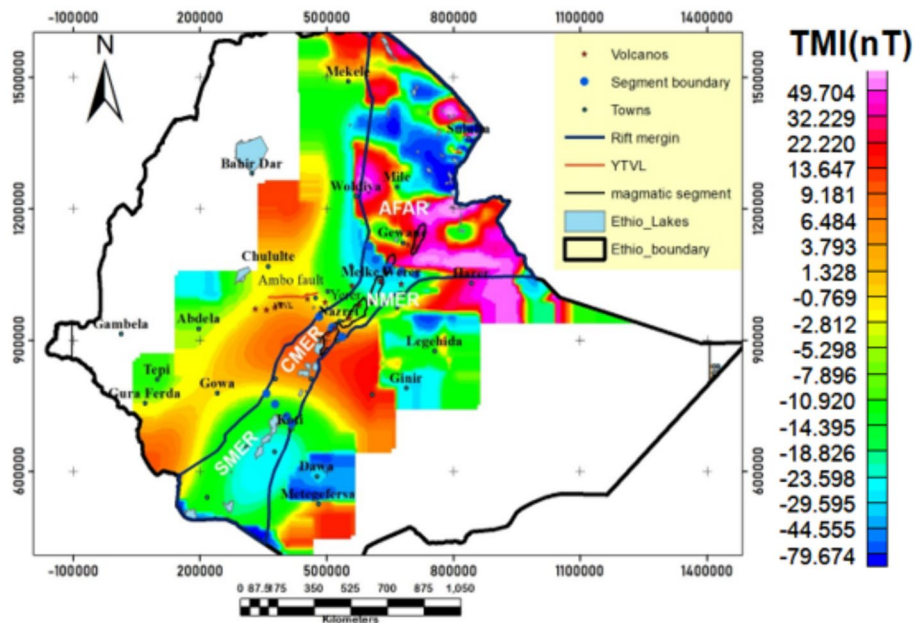

Fig. 5 Total magnetic intensity (TMI) anomaly map of the ERS and its surroundings

where I and D are the inclination and declination of core field, (u, v) is the wavenumber corresponding to the (x, y) directions, respectively, $\theta = \arctan(u/v)$ and $i^2 = 1$.

Depth to centroid (Z_o), top limit (Z_t) and base depth (Z_b)

The magnetic source's depth is determined using the techniques developed by Spector and Grant (1970). This approach establishes a link between the magnetic anomaly spectrum and the depth of magnetic sources in the wave number/frequency domain (Bello et al. 2018) and is used to calculate the depth to the top (Z_t) of the magnetic source and its centroid depth (Z_o). To do this, the data were first transformed from the time domain to the frequency domain using the Fast Fourier transform method and the magnetic source depth estimates were then calculated using the slope of the log of power spectrum of magnetic anomaly data.

To carry out spectral analysis, the study area was divided into 105 overlapping blocks, each block covering a square place of 200 km by 200 km, which constitute a square grid of 36-by-36 data and a total of 1302 data points. The centre of each square area is represented with a cross symbol (Fig. 6). The assessment was carried out using the Oasis Montaj model 7.0.1 computer software (Montaj 2007). Geosoft's Oasis Montaj is a powerful processing and mapping software program application for
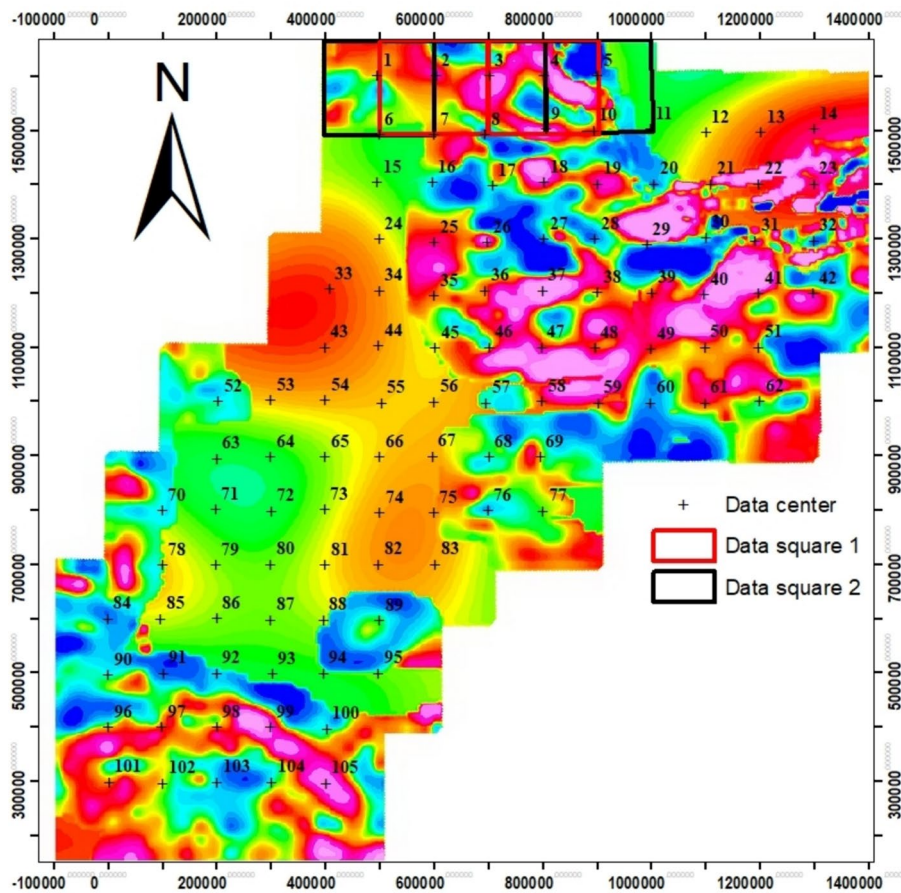

Fig. 6 TMI map showing the 105 square windows (from C1 to C105; 200 km by 200 km each). 50% overlapping of adjacent blocks was used for power spectral analysis

mineral exploration, oil and gas exploration, and Earth science investigations collectively with environmental initiatives and Unexploded Ordnance (UXO) detection.

In doing this, each rectangular area becomes gridded at the default cell size using minimum curvature. The gridded data was further processed with the useful resource of magmap one-step filtering Oasis Montaj software program to reduce to magnetic pole (RTP). The RTP grid is converted to a frequency domain by using Fourier transformation (FFT2 grid pre-processing technique) and calculating the radial average spectrum. This method determines the depth to the top (Z_t), center Z_o), and basal depths (Z_b) (expect as CPD) of the magnetic source (Okubo et al. 1985).

According to Njeudjang et al. (2020), Kasidi and Nur (2012), CPD (Z_b) may be obtained in three steps. First of all, the depth to the Centroid (Zo) of the magnetic deliver is estimated from the slope of the longest wavelength part of the spectrum (this is the upper part of Fig. 8) using the subsequent equation:

$$\ln\left[\frac{P\,(S)^{\frac{1}{2}}}{/S/}\right] = \ln A - 2\pi\,/s/Zo \tag{2}$$

where *P(s)* is the radially averaged power spectrum of the anomaly, /s/ is the wave number, and A is a constant.

Second, the depth to the top limit (Z_t) of the magnetic source is anticipated from the slope of the top-frequency component section of the energy spectrum (this is the lower part of Fig. 8) and the usage of the subsequent mathematical equation:

$$\mathrm{Ln}\left(P\,(S)^{\frac{1}{2}}\right) = \ln B - 2\pi\,/s/Z_t \tag{3}$$

where B is the sum of constants independent of /s/.

Finally, the base depth (Z_b) (assumed to represent the required CPD) in each window is calculated from the mathematical equation of

$$Z_b = 2Z_o - Z_t \tag{4}$$

Heat flow and temperature gradient

Heat flux or thermal flux, so often known as heat flow density, is the transfer of heat energy from one place to another per unit time per unit cross-sectional area over which heat transfer takes place (Schaschke 2014). The rate of heat flowing out of the Earth is calculated with the aid of the formula below (International Heat Flow Commission 2008):

$$Q_Z = -\mathrm{K}\frac{d\mathrm{T}}{d\mathrm{Z}} = -\,\mathrm{K}\,\frac{Q_c}{Z_b} \tag{5}$$

in which Q_z is the heat flow, Q_c is the Curie temperature, **K** is thermal conductivity, and dt is the temperature difference over a given depth interval dz. The negative sign in the formula shows that heat flow moves from higher-temperature to lower-temperature regions.

This heat flow equation assumes that there are no heat sources (heating elements, such as radiation elements) or heat sinks between the earth surface and the Curie point depth (Odidi et al. 2020). It also assumes that the temperature at the sea-level surface ($Zo = 0$) is 0 ℃ (Odidi et al. 2020) and that the temperature gradient is constant up to the Curie point depth. According to Li et al. (2017) average continental and oceanic crust thermal conductivities were estimated as $K = 2.5\,\text{W}(\text{m}^\circ\text{C})^{-1}$ and $K = 2.0\,\text{W}(\text{m}^\circ\text{C})^{-1}$, respectively. These conductivity values are matched with those of granite and basalt.

Geothermal gradient is the rate of temperature variation with respect to increasing depth into the Earth's interior. The Geothermal gradient (dT/dZ) of the Earth at CPD (Z_b) can be estimated as

$$\Delta T \ = \ \frac{dT}{dZ} \ = \ \frac{Q_z}{Z_b} \ = \ \frac{580^\circ C}{Z_b} \tag{6}$$

where Q_z is the Curie temperature having an approximate value of 580 ℃ (Ross et al. 2006) and Z_b is the Curie depth. This temperature is assumed to correspond to the Curie Depths, where magnetic minerals lose all their magnetization.

It is an accepted observation that the temperature within the crust increases with depth due to the upward heat flow from the much warmer mantle. Further away from tectonic plate boundaries, the temperature rises by approximately 25–30 ℃/km (72–87 ℉/mi) of depth in most of the globe (Georgsson and Fridleifsson 2013).

Results and discussion

Selecting the correct window length of the study area could be very critical to decrease errors at some stage in the determination of Z_o and Z_t through the usage of the average radial spectrum. Tanaka et al. (1999) used a 200 km × 200 km window length and Blakely (1988) used 120 km × 120 km to estimate the power density spectra for every area. If the curie depth has bases deeper than L/2π, L being the window size length, it will no longer be accurately resolved by the spectral method (Shuey et al. 1977; Khojamli et al. 2016). In the current study, windows of 200 km × 200 km (overlapped 50%) were used to attain intermediate resolution, avoiding regional effects (Fig. 6). The 2D power spectrum of aeromagnetic data for every block was then computed using the Oasis Montaj 7.0.1. software program with Fast Fourier transform (FFT) method. The RTP map of the ERS thus derived suggests that the magnetic field of the study area can be broken into two important anomaly regions: (1) the MER (subdivided into NMER, CMER and SMER) characterized by a lower regional magnetic field that varies unevenly and (2) the Afar region characterized by higher magnetic anomalies (Fig. 5).

The TMI anomaly map manifests wide spatial variations (−79.67nT to 49.70 nT) that imply different sources, depths and compositions. The map shows that the maximum of the anomalies is arranged in the N–S direction with sharp and clean gradients. The map further indicates that a smooth transition among segment boundaries (e.g., NMER-Afar boundary). These different tendencies simply display that these locations are subjected to some kind of tectonic force over its geological history (Keranen and Klemperer 2008). Negative anomalies are found in north and eastern Afar, northeast NMER Southern Rift and adjacent eastern highlands.
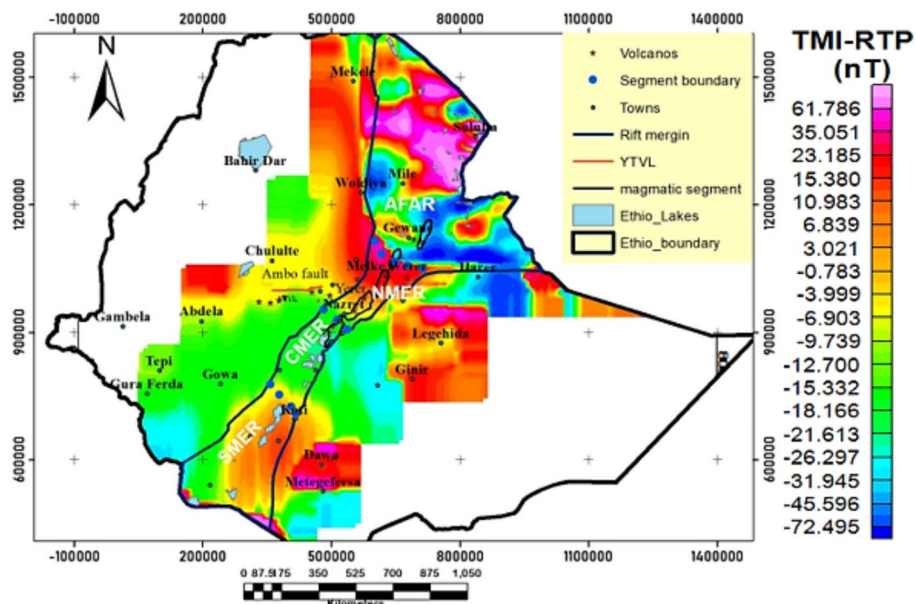
Fig. 7 TMI reduced-to-pole (TMI–RTP) anomaly map of the Ethiopian Rift System (ERS) and adjoining areas
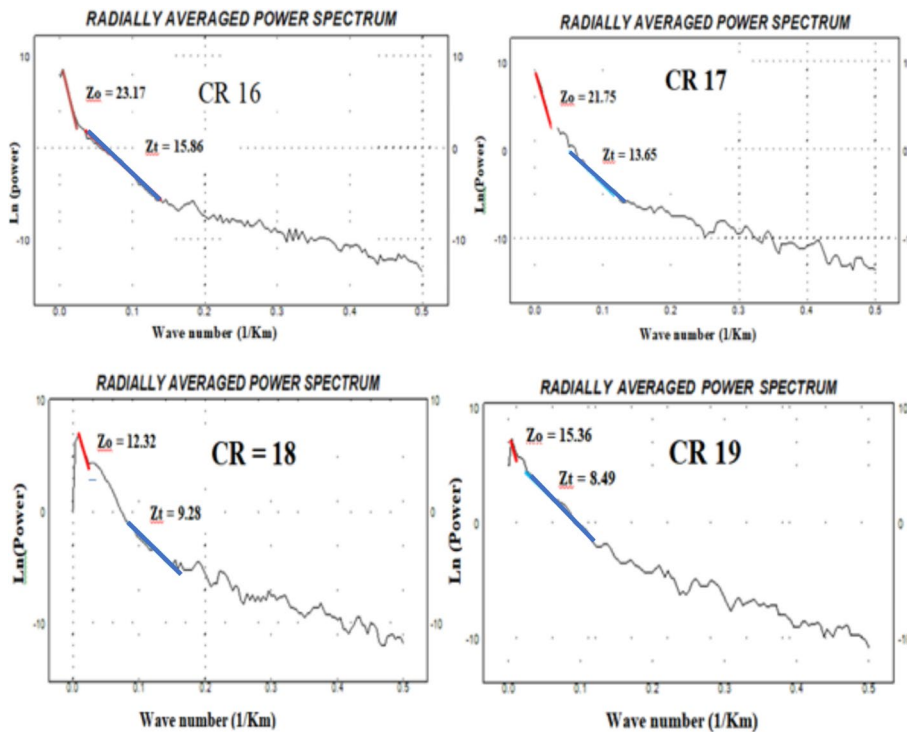
Fig. 8 Example of radially averaged power spectrum used for estimating CPD of four zones (CR 16–CR 19). Only the long-wavelength domain of the spectrum is used for CPD determination. Red lines and blue lines, respectively, are indicating the spectrum zone used to calculate the depth to the top (Z_t) and to determine the centroid (Z_o). The high-frequency region above the wavenumber of 0.2/km seems to be noise

In Fig. 6, the RTP magnetic anomaly map of the study area was sectioned into 105 blocks, with 50% overlap with a grid of 200 km-by-200 km area. Radially averaged power spectrum analysis was carried out on the processed aeromagnetic data and the centres of the blocks are marked by a plus (+) sign. In each region, the power spectrum was obtained using Oasis Montaj 7.0.1 software program to determine the depths of the magnetic sources at the top (Z_t) and at the centroid (Z_o). The depth to the top (Z_t) was estimated using Eq. 1, while the depth to the centroid (Z_o) using Eq. 2, and finally, the CPD was calculated using Eq. 3.

As pointed out by Soengkono et al. (2016), the total magnetic field anomaly pattern caused by the geothermal system is much less bipolar; however, positive anomalies turn out to be dominant. Hence, it is essential to be continually conscious of this contradictory phenomenon (negative magnetization developing positive anomalies). In this low geomagnetic latitude (at equatorial zones), hydrothermally demagnetized rocks are to be identified from positive anomalies, not from negative anomalies. Thus, to resolve this contradiction and produce a strong anomaly map, TMI is remapped by means of the usage of the reduced-to-pole method. The determined TMI–RTP magnetic anomaly map is given in Fig. 7.

Figure 7 exhibits a series of positive and negative magnetic anomalies over the ERS and on the plateaus close to the rift margins. The RTP magnetic anomaly values range from −72.495 nT to 61.786 nT. This wide variation in magnetic anomaly values indicates differences in the source, depths and compositions of the anomalous bodies. Negative magnetic anomalies are observed over the CMER and south Afar which also extend southwards to the eastern part of the South-eastern Ethiopian plateau. These low anomalies could arise from rock demagnetization by means of relatively higher thermal supply attributed to greater crustal thinning or shallow igneous intrusions or a combination of both causes. It is also possible that part of the regional negative anomaly could derive from large-scale magmatic underplating at the crust–mantle boundary below the principal active volcanic centres. Identical end results were found by Mikus et al. (2007) and Tiberi et al. (2005) using gravity anomalies and seismic wave speeds. On the other hand, positive anomalies are located over northern and central Afar, NMER and the eastern sector of SMER and adjacent plateau.

Figure 8 shows the sample graphs of the logarithms of the spectral energies for plots of blocks CR16 to CR19. The determined values of the Curie point depth for CR16, CR17, CR18, and CR19, respectively, are $Z_b = 30.48$, $Z_b = 29.85$, $Z_b = 15.36$, and $Z_b = 22.23$. On the logarithm of power against the wavenumber graph, red lines are corresponding to Z_o and blue traces are associated with Z_t. The part of spectra used for the determination of Z_o and Z_t are for the most part less than a wave number of 0.1/km due to the fact it is these regions in which the CPD is defined (De Ritis et al. 2013; Salem et al. 2014). The high-frequency region above the wavenumber of 0.2/km seems to be noise. An illustration of the determined values of Curie point depth, geothermal gradient and heat flow for the 105 (50% overlapped) blocks is given in Appendix 1.

The Curie Point Depth along the Ethiopia Rift System (ERS) and the rift margins (northwest and southeast of the rift) are mapped and shown in Fig. 9. The Curie Point Depths range from 8.85 km to 55.85 km, with a mean value of 27.44 km. Lower CPD is located in the areas between Mille and Gewane (Afar), between Adama (Nazret) and
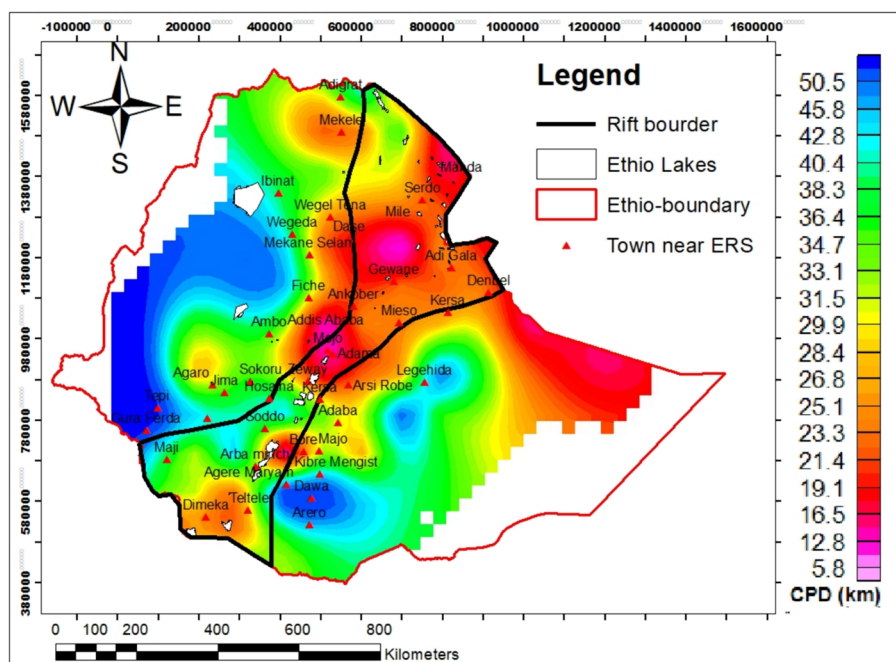
Fig. 9 Curie point depth (CPD) of the ethiopian rift system (ERS), the rift margins, the adjacent plateaus and low-lying regions

Yerer (NMER) and between Wengo and Koti (SMER). According to Tanaka et al. (1999), CPD less than 15 km indicate that the area is a volcanic and geothermal zone, since CPD is highly reliant on geologic setting. On the other hand, higher CPD is found outside the ERS in the areas between Ginir and Dawa (southeastern plateau), between Bahir Dar and Chululte (northwestern plateau) and between Gambela and Tepi (southwestern highlands). The region of lower Curie depths along the western rift margin (Afar area) and NMER may be the result of volcanism and crustal extension (Li et al. 2017). The areas with shallow CPD and high geothermal gradient mapped in central Afar, NMER and CMER can be correlated with the identified geothermal potential regions (Figs. 9 and 10). The geothermal sites displayed in Fig. 2 are usually found in low CPD areas, with the exception of the Aluto, Butajira, Shala, Abijata, and Wendo Genet areas which are found at high CPD (Fig. 9). It is reasonable to believe that the heat source for these regions is very deep; because these geothermal zones are positioned, such that they might have been formed by magma rising from deeper sources that rose through recent rift faults. The presence of low CPD around Arba Minch and Dimeka areas suggests that the areas are to be considered as geothermal potential locations, although no surface geothermal manifestation is apparent in these areas. The eastern portion of Afar around Manda and Serdo towns has the lowest curie depth of any location in the ERS (< 15 km). These regions also indicate relatively greater potential for geothermal energy beyond what is already determined. Furthermore, the regions from Adi Kela to the northwest boundary of the Afar rift on the Mille side which exhibit low CPD are suggested to have high geothermal energy.

A temperature gradient is a physical quantity that describes in which direction and at what rate the temperature modifications vary the most rapidly around a selected area.
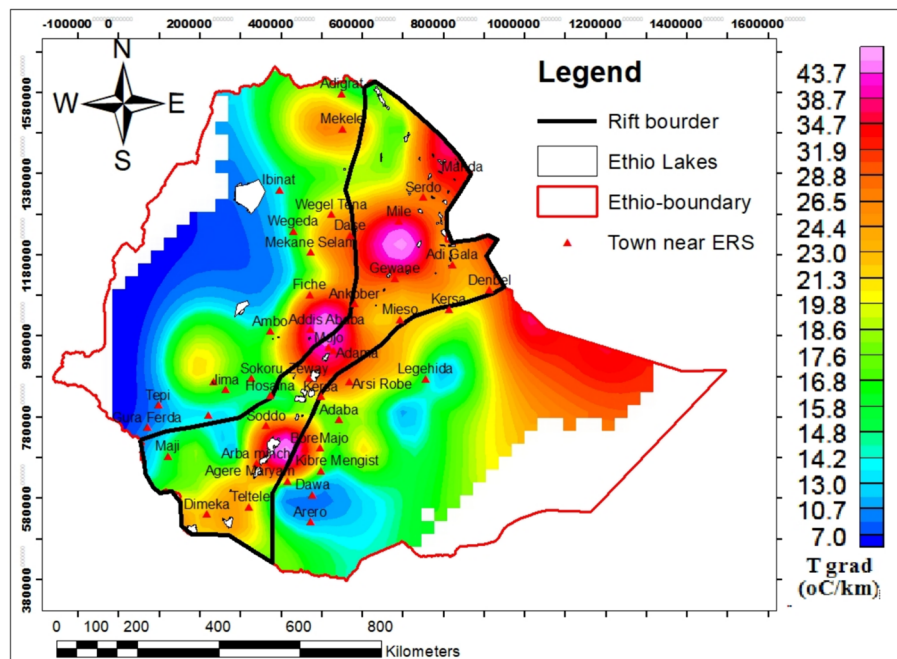
Fig. 10 Temperature gradient map of the ERS derived from the CPD and Curie temperature at 580 ℃

The geothermal gradient anomaly map of the ERS (Fig. 10) shows that the geothermal gradient values range between 10.38 and 65.54 °C/km with a mean value of 25.62 °C/km. The temperature gradient (Tgrad) is calculated using Eq. (5) and all calculated values are indexed in Table 1. In large parts of the study area, particularly in the ERS, the determined Tgrad value exceeds the worldwide average of 30 oC∕km (Georgsson and Fridleifsson 2013). As an example, areas around Gewane (Afar), Adama (NMER) and Koti (SMER) exceed this value. The intermediate temperature gradient areas are located in northern Ethiopia around Mekele, south Ethiopia near Bale-Robe to Ginir, west of the ERS around Abdela and around Dimeka (SMER). Low gradient regions are located between Chululte and Bahir Dar (northwest Ethiopia), Gowa (west of the SMER), Dawa and Metegefersa (southeast of SMER) and Ginir (south Ethiopia). These low gradient areas also systematically show large CPD values. Low-temperature gradient values of 20 °C/km to 25 °C/km and low CPD value have been found in the SMER around Abaya basin and Dimeka town. These values might be due to thick Quaternary sedimentary cover in those areas; a result in line with that of Kebede and Mammo (2021).

Heat flow (W/m^2) is the rate of thermal energy flow per unit surface area of heat transfer surface. The quantity of heat flow calculated and given in Fig. 11 has been obtained using an average thermal conductivity of 2.5 W/m °C and the temperature gradient over a given depth interval Zb (Curie point depths) using Eq. (4). As revealed on the map (Fig. 11), ERS is characterised by anomalously higher heat flow compared to the Ethiopian plateaus. According to the map, maximum heat flow is located in south central Afar, northern CMER and in SMER northeast of Lake Abaya. These anomalous heat flow areas have been defined by different authors as magmatically active areas (Mickus et al. 2007; Keranen et al. 2004; Keller et al. 2004; Magaire et al. 2003). The determined heat flow over ERS ranges from 25.96 mWm^{-2} to 163.84 mWm^{-2}, with an average value of

Table 1 Showing the first 30 (CR1–CR30) estimated values of CPD, geothermal gradients, and heat flow (full data is found in Appendix 1)

CR	XUTM (m)	YUTM (m)	Zo (km)	Zt (km)	CPD (km)	Tgrad °C (/km)	Hflow (mW/m²)
1	500000	1600000	22.85	14.21	31.49	18.41855	46.04636
2	600000	1600000	30.36	17.26	43.46	13.34561	33.36401
3	700000	1600000	23.85	23.7	24	24.16667	60.41667
4	800000	1600000	17.16	9.3	25.02	23.18145	57.95364
5	900000	1600000	11.14	9.13	13.15	44.10646	110.2662
6	500000	1500000	14.93	7.85	22.01	26.35166	65.87915
7	600000	1500000	17.72	10.74	24.7	23.48178	58.70445
8	700000	1500000	24	12.59	35.41	16.37955	40.94888
9	800000	1500000	14.03	13.08	14.98	38.71829	96.79573
10	900000	1500000	10.84	8.09	13.59	42.67844	106.6961
11	1000000	1500000	8.2	3.14	13.26	43.74057	109.3514
12	1100000	1500000	14.12	4.46	23.78	24.39024	60.97561
13	1200000	1500000	10.5	7.46	13.54	42.83604	107.0901
14	1300000	1500000	9.88	8.6	11.16	51.97133	129.9283
15	500000	1400000	22.95	11.63	34.27	16.92442	42.31106
16	600000	1400000	23.17	15.86	30.48	19.02887	47.57218
17	700000	1400000	21.75	13.65	29.85	19.43049	48.57621
18	800000	1400000	12.32	9.28	15.36	37.76042	94.40104
19	900000	1400000	15.36	8.49	22.23	26.09087	65.22717
20	1000000	1400000	16.83	10.64	23.02	25.19548	62.98871
21	1100000	1400000	27.82	20.68	34.96	16.59039	41.47597
22	1200000	1400000	10.45	11.83	9.07	63.94708	159.8677
23	1300000	1400000	7.37	1.56	13.18	44.00607	110.0152
24	500000	1300000	20.49	11.75	29.23	19.84263	49.60657
25	600000	1300000	17.71	10.07	25.35	22.87968	57.19921
26	700000	1300000	22.99	24.35	21.63	26.81461	67.03652
27	800000	1300000	25.14	27.62	22.66	25.59576	63.98941
28	900000	1300000	12.42	10.33	14.51	39.97243	99.93108
29	1000000	1300000	15.13	5.33	24.93	23.26514	58.16286
30	1100000	1300000	7.58	3.42	11.74	49.40375	123.5094

64.04 mWm^{-2}. According to the heat flow map of the International Heat Flow Commission (IHFC 2008), the East African region is characterized by values ranging from 60 to 80 mWm^{-2} compared to the worldwide mean heat flow is 68.3 mWm^{-2} (Li et al. 2017). The heat flow map, Fig. 11 positively displays that the areas between Gewane and Mille (central Afar), between Iteya and Ankober (NMER) and between Kele and Koti (>80 mWm^{-2}) exceed the average heat flow value. Based on this observation, high heat flow areas can be correlated with geothermal areas. In addition to the potential geothermal locations outlined in Fig. 2, the regions from Mille to Gewane (in Afar), Iteya to Ankober (NMER), and Kele to Koti (SMER) have significantly high heat flow (>120 mWm^{-2}) and might be considered as geothermal prospect areas (Fig. 11).
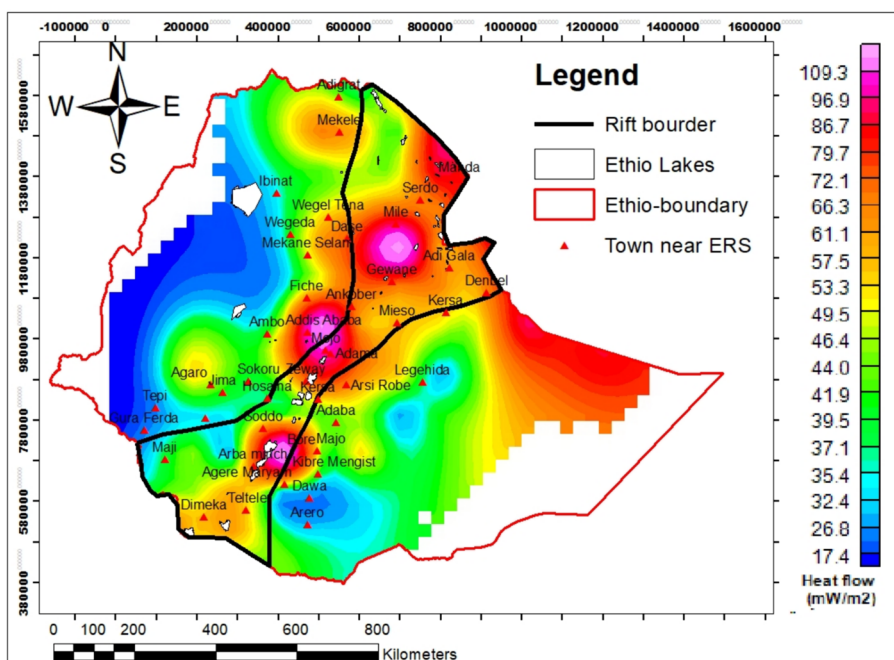
Fig. 11 Heat flow map of ERS using an average geothermal conductivity of $K = 2.5 W/m^oC$

Conclusions

This study has revealed that, in the Ethiopian Rift System (ERS), the CPD range from 8.85 km to 55.85 km, with a mean value of 27.44 km. The regions of lower CPD extend from Mille to Gewane (Afar), Adama (Nazret) to Yerer (NMER) and Wengo to Koti (SMER). Most of the lower CPD (< 20 km) in the ERS are found nearby Mille and Adama (Nazret) localities. The thermal gradient values obtained for these regions range between 10.38 and 65.53 °C/km with a mean value of 25.62 °C/km (Fig. 8). The thermal gradient is higher especially in the Gewane (Afar) area, Adama (Nazret) (NMER) and Koti (SMER) vicinity and is minimum in most of the west, southwest and south areas of the Ethiopian plateaus. On the other hand, the heat flow over the ERS varies from 25.96 mWm^{-2} to 163.84 mWm^{-2}, with a mean value of 64.04 mWm^{-2}. The heat flow values from Gewane to Mille (in central Afar), Iteya to Sendafa (NMER) and Kele to Koti (between CMER and SMER boundary) exceed the mean world heat flow value.

The overview of prior investigations reveals that CPDs change depending on the geological environment (Tanka et al. 1999). Accordingly, our results indicate that the CPD are found to be shallower than ∼ 12 km in volcanic and geothermal manifestation regions of the rift axis, 20–25 km near the rift borders and deeper than 35 km on the eastern and western highlands with the exception of the areas in the transition zone between the SMER and CMER. This exception could be due to higher crustal thickness (Keranen et al. 2009) and the Goba–Bonga cross rift structure.

The regions with the shallowest CPDs (< 12 km), which are accompanied by high heat flow (> 120 mW/m^{-2}) and thermal gradient (> 40 oC/km) that fall near Adama, Mille, and Koti localities, are identified as suitable prospects for further geothermal investigation. Potential exploitation of the enormous geothermal resource from these localities has the ability to boost the currently small (7.3 MW) contribution to the national grid and become a noticeable alternative for alleviating the country's high-power demand.

Appendix 1

CR	XUTM (m)	YUTM (m)	Z_o (km)	Z_t (km)	CPD (km)	Tgrad (ºC/km)	Heat flow (mW/m^2)
1	500000	1600000	22.85	14.21	31.49	18.41855	46.04636
2	600000	1600000	30.36	17.26	43.46	13.34561	33.36401
3	700000	1600000	23.85	23.7	24	24.16667	60.41667
4	800000	1600000	17.16	9.3	25.02	23.18145	57.95364
5	900000	1600000	11.14	9.13	13.15	44.10646	110.2662
6	500000	1500000	14.93	7.85	22.01	26.35166	65.87915
7	600000	1500000	17.72	10.74	24.7	23.48178	58.70445
8	700000	1500000	24	12.59	35.41	16.37955	40.94888
9	800000	1500000	14.03	13.08	14.98	38.71829	96.79573
10	900000	1500000	10.84	8.09	13.59	42.67844	106.6961
11	1000000	1500000	8.2	3.14	13.26	43.74057	109.3514
12	1100000	1500000	14.12	4.46	23.78	24.39024	60.97561
13	1200000	1500000	10.5	7.46	13.54	42.83604	107.0901
14	1300000	1500000	9.88	8.6	11.16	51.97133	129.9283
15	500000	1400000	22.95	11.63	34.27	16.92442	42.31106
16	600000	1400000	23.17	15.86	30.48	19.02887	47.57218
17	700000	1400000	21.75	13.65	29.85	19.43049	48.57621
18	800000	1400000	12.32	9.28	15.36	37.76042	94.40104
19	900000	1400000	15.36	8.49	22.23	26.09087	65.22717
20	1000000	1400000	16.83	10.64	23.02	25.19548	62.98871
21	1100000	1400000	27.82	20.68	34.96	16.59039	41.47597
22	1200000	1400000	10.45	11.83	9.07	63.94708	159.8677
23	1300000	1400000	7.37	1.56	13.18	44.00607	110.0152
24	500000	1300000	20.49	11.75	29.23	19.84263	49.60657
25	600000	1300000	17.71	10.07	25.35	22.87968	57.19921
26	700000	1300000	22.99	24.35	21.63	26.81461	67.03652
27	800000	1300000	25.14	27.62	22.66	25.59576	63.98941
28	900000	1300000	12.42	10.33	14.51	39.97243	99.93108
29	1000000	1300000	15.13	5.33	24.93	23.26514	58.16286
30	1100000	1300000	7.58	3.42	11.74	49.40375	123.5094
31	1200000	1300000	8.04	5.06	11.02	52.63158	131.5789
32	1300000	1300000	7.2	5.55	8.85	65.53672	163.8418
33	500000	1200000	14.03	4.33	23.73	24.44164	61.10409
34	600000	1200000	15.24	12.79	17.69	32.78689	81.96721
35	700000	1200000	20.88	31.11	10.65	54.46009	136.1502
36	800000	1200000	17.53	8.81	26.25	22.09524	55.2381
37	900000	1200000	14.36	8.72	20	29	72.5

Hilemichaeil *et al. Geothermal Energy* (2024) 12:13

Page 18 of 22

CR	XUTM (m)	YUTM (m)	Z_o (km)	Z_t (km)	CPD (km)	Tgrad (°C/km)	Heat flow (mW/m²)
38	1000000	1200000	8.42	4.99	11.85	48.94515	122.3629
39	1100000	1200000	12.55	9.85	15.25	38.03279	95.08197
40	1200000	1200000	17.06	13.4	20.72	27.99228	69.98069
41	1300000	1200000	17.05	8.14	25.96	22.34206	55.85516
42	400000	1200000	28.97	12.33	45.61	12.71651	31.79127
43	400000	1100000	29.4	11.43	47.37	12.24404	30.61009
44	500000	1100000	20.14	11.4	28.88	20.0831	50.20776
45	600000	1100000	15.18	9.38	20.98	27.64538	69.11344
46	700000	1100000	16.69	8.55	24.83	23.35884	58.3971
47	800000	1100000	20.35	18.14	22.56	25.70922	64.27305
48	900000	1100000	19.53	14.19	24.87	23.32127	58.30318
49	1000000	1100000	15.07	13.61	16.53	35.08772	87.7193
50	1100000	1100000	13.84	13.03	14.65	39.59044	98.97611
51	1200000	1100000	24.29	6.66	41.92	13.83588	34.58969
52	300000	1000000	24.67	11.42	37.92	15.29536	38.2384
53	400000	1000000	23.13	12.01	34.25	16.93431	42.33577
54	500000	1000000	20.5	30.57	10.43	55.60882	139.0221
55	600000	1000000	19.03	13.17	24.89	23.30253	58.25633
56	700000	1000000	19.94	14.9	24.98	23.21857	58.04644
57	800000	1000000	17.81	6.36	29.26	19.82228	49.55571
58	900000	1000000	23.69	17.8	29.58	19.60784	49.01961
59	1000000	1000000	13.31	11.24	15.38	37.71131	94.27828
60	1100000	1000000	14.6	9.93	19.27	30.0986	75.2465
61	1200000	1000000	11.81	7.74	15.88	36.52393	91.30982
62	200000	1000000	22.79	12.43	33.15	17.49623	43.74057
63	200000	900000	21.29	16.88	25.7	22.56809	56.42023
64	300000	900000	20	5.62	34.38	16.87027	42.17568
65	400000	900000	27.94	26	29.88	19.41098	48.52744
66	500000	900000	23.51	30.88	16.14	35.93556	89.83891
67	600000	900000	17.66	12.98	22.34	25.9624	64.906
68	700000	900000	18.97	12.04	25.9	22.39382	55.98456
69	800000	900000	30.26	11.13	49.39	11.74327	29.35817
70	100000	800000	31.38	6.91	55.85	10.38496	25.9624
71	200000	800000	23.72	4.01	43.43	13.35482	33.38706
72	300000	800000	29.06	18.29	39.83	14.56189	36.40472
73	400000	800000	43.36	40.49	46.23	12.54597	31.36491
74	500000	800000	33.74	32.76	34.72	16.70507	41.76267
75	600000	800000	20.25	10.04	30.46	19.04137	47.60341
76	700000	800000	37.39	25.08	49.7	11.67002	29.17505
77	800000	800000	22.71	10.59	34.83	16.65231	41.63078
78	100000	700000	27.61	14.25	40.97	14.1567	35.39175
79	200000	700000	26.1	20.73	31.47	18.43025	46.07563
80	300000	700000	30.35	15.88	44.82	12.94065	32.35163
81	400000	700000	14.9	19.69	10.11	57.36894	143.4224
82	500000	700000	19.62	7.09	32.15	18.04044	45.10109
83	600000	700000	21.36	15.83	26.89	21.56936	53.92339
84	100000	600000	24.57	14.1	35.04	16.55251	41.38128
85	200000	600000	23.4	15.17	31.63	18.33702	45.84255
86	300000	600000	31.31	38.94	23.68	24.49324	61.23311
87	400000	600000	34.37	14.4	54.34	10.67354	26.68384

CR	XUTM (m)	YUTM (m)	Z_o (km)	Z_t (km)	CPD (km)	Tgrad (^{o}C/km)	Heat flow (mW/m^2)
88	500000	600000	32.74	11.32	54.16	10.70901	26.77253
89	0	500000	20.66	10.22	31.1	18.64952	46.62379
90	0	500000	22.35	16.35	28.35	20.45855	51.14638
91	100000	500000	15.87	13.58	18.16	31.93833	79.84581
92	200000	500000	19.25	11.54	26.96	21.51335	53.78338
93	300000	500000	18.57	13.19	23.95	24.21712	60.5428
94	400000	500000	23.57	11.62	35.52	16.32883	40.82207
95	500000	500000	25.46	8.73	42.19	13.74733	34.36833
96	0	400000	21.69	22.32	21.06	27.54036	68.8509
97	100000	400000	21.84	10.49	33.19	17.47514	43.68786
98	200000	400000	25.19	12	38.38	15.11204	37.78009
99	300000	400000	25.94	11.01	40.87	14.19134	35.47835
100	400000	400000	22.43	13.26	31.6	18.35443	45.88608
101	0	300000	18.57	14.9	22.24	26.07914	65.19784
102	100000	300000	22.32	22.7	21.94	26.43573	66.08933
103	200000	300000	29.46	11.41	47.51	12.20796	30.51989
104	300000	300000	22.09	11.89	32.29	17.96222	44.90554
105	400000	300000	22.68	10.21	35.15	16.50071	41.25178

Abbreviations

CMER	Central Main Ethiopia Rift
CPD	Curie point depth
EARS	East Africa Rift system
ERS	Ethiopia Rift System
FFT	Fast Fourier transform
IGRF	International Geomagnetic Reference field
IHFC	International Heat Flow Commission
MER	Main Ethiopia Rift
MT	Magnetotelluric
NMER	North Main Ethiopia Rift
RTP	Reduction to Pole
SMER	South Main Ethiopia Rift
TMI	Total magnetic intensity
TMS	Tectono-magmatic segments
UXO	Unexploded ordnance
WDMAM	World Digital Magnetic Anomaly Map
WFB	Wonji fault belt

Availability of data and materials
The data sets generated and/or analyzed during the current study are available in the World Digital Magnetic Anomaly Map V2 (WDMAM) repository, http://www.wdmam.org/download.php.

Declarations

Ethics approval and consent to participate
This research did not involve human participants and/or animals.

Competing interests
The authors declare that they have no competing interests.

References

Abbate E, Sagri M. Volcanites of Ethiopian and Somali Plateaus and major tectonic lines. Atti Convegni Acc Lincei Roma. 1980;47:219–27.

Abbate E, Piero B, Mario S. Geology of Ethiopia: a review and geomorphological perspectives. Res Gate. 2015;2:33–64. https://doi.org/10.1007/978-94-017-8026-1_2.

Abebe T, Mazzarini F, Innocenti F, Manetti P. The Yerer-Tullu Wellel Volcanotectonic lineament: a transtensional structure in central Ethiopia and the associated magmatic activity. J Afr Earth Sci. 1998;26:135–50.

Adhana AT. The occurrence of a complete continental rift type of volcanic rocks suite along the Yerer-Tullu Wellel Volcano Tectonic Lineament, Central Ethiopia. J Afr Earth Sci. 2014;99:374–85.

Amanu BZ. Strengthening of the geothermal sector in Ethiopia. Reykjavik: UNU-GTP, Orkustofnun; 2018. pp. P633–654. https://orkustofnun.is/gogn/unu-gtp-report/UNU-GTP-2018-31.pdf.

Baker BH, Mohr PA, Williams LAJ. Geology of the eastern rift system of Africa. Boulder: Geological Society of America; 1972. https://doi.org/10.1130/SPE136-p1.

Barberi F, Ferrara G, Santacroce R, Varet J. Structural evolution of the Afar triple junction. In: Pilger A, Rosler A, editors. Afar depression of Ethiopia. Inter-Union Commission on Geodynamics, Scientific Report. Stuttgart: Nagele Obermillar; 1975. p. 38–54.

Bastow ID, Stuart GW, Kendall JM, Ebinger CJ. Upper mantle seismic structure in a region of incipient continental breakup: Northern Ethiopian rift. Geophys J Int. 2005;162(2):479–93. https://doi.org/10.1111/j.1365246X.2005.02666.x.

Bellahsen N, Faccenna C, Funiciello F, Daniel JM, Jolivet L. Why did Arabia separate from Africa? Insights from 3-D laboratory experiments. Earth Planet Sci Lett. 2003;216:365–81.

Bello S, Udensi EE, Salako K, Adetona AA. Determination of depth to magnetic basement using spectral analysis of aeromagnetic data over biu plateau basalt and yola sub-basin, North East Nigeria. 2018. http://repository.futminna.edu.ng:8080/jspui/handle/123456789/6461.

Beyene A. Evolution of the Afar Depression from orbital optical and radar, Ethiopia. Ph.D. Dissertation, The University of Texas at Dallas. 2004; 138p

Blakely R. Curie temperature isotherm analysis and tectonic implications of aeromagnetic data from Nevada. J Geophys Res. 1988;93:11817–32.

Boccaletti M, Bonini M, Mazzuoli R, Abebe B, Piccardi L, Tortorici L. Quaternary oblique extensional tectonics in the Ethiopian Rift (Horn of Africa). Tectonophysics. 1998;287:97–116.

Boccaletti M, Mazzuoli R, Bonini M, Trua T, Abebe B. Plio-Quaternary volcano-tectonic activity in the northern sector of the Main Ethiopian Rift (MER): relationships with oblique rifting. J Afr Earth Sc. 1999;29(4):679–98. https://doi.org/10.1016/S0899-5362(99)00124-4.

Bonin A, Bellemain E, Eidesen PB, Pompanon F, Brochmann C, Taberletet P. How to track and assess genotyping errors in population genetics studies. Mol Ecol. 2004;13:3261–73. https://doi.org/10.1111/j.1365-294X.2004.02346.x.

Bonini M, Corti G, Innocenti F, Manetti P, Mazzarini F, Abebe T, Pecskay Z. Evolution of the Main Ethiopian Rift in the frame of Afar and Kenya rifts propagation. Tectonics. 2005;24:1–21. https://doi.org/10.1029/2004TC001680.

Casey M, Ebinger C, Keir D, Gloaguen R, Mohamed F. Strain accommodation in transitional rifts: Extension by magma intrusion and faulting in Ethiopian rift magmatic segments. Geol Soc Lond Special Publ. 2006;259:143–63. https://doi.org/10.1144/GSL.SP.2006.259.01.13.

Chorowicz J, Collet B, Bonavia F, Korme T. NW to NNW extension direction in the Ethiopian Rift deduced from the orientation of tension fractures and fault slip analysis. Geol Soc Am Bull. 1994;105:1560–70.

Cooper GRJ, Cowan DR. Differential reduction to the pole. Comput Geosci. 2005;31:989–99. https://doi.org/10.1016/j.cageo.2005.02.005.

Corti G. Continental rift evolution: from rift initiation to incipient break-up in the main Ethiopian Rift, East Africa. Earth Sci Rev. 2009;96(1):1–53.

Corti G, Philippon M, Sani F, Keir D. Re-orientation of the extension direction and pure extensional faulting at Oblique Rift Margins: comparison between the Main Ethiopian Rift and laboratory experiments. Terra Nova. 2013;25(5):396–404. https://doi.org/10.1111/ter.12049.

Corti G, Sani F, Agostini S, Philippon M, Sokoutis D, Willingshofer E. Off-axis volcano-tectonic activity during continental rifting: insights from the transversal Goba-bonga lineament, Main Ethiopian Rift (East Africa). Tectonophysics. 2018;728:75–91. https://doi.org/10.1016/j.tecto.2018.02.011.

Corti G, Maestrelli D, Sani F. Large-to local-scale control of Preexisting structures on continental rifting: examples from the Main Ethiopian Rift, East Africa. Front Earth Sci. 2022;10:1–18. https://doi.org/10.3389/feart.2022.808503.

Courtillot V, Davaille A, Besse J, Stock J. Three distinct types of hotspots in the Earth's mantle. Earth Planet Sci Lett. 2003;205:295–308.

De Ritis R, Ravat D, Ventura G, Chiappini M. Curie isotherm depth from aeromagnetic data constraining shallow heat source depths in the central Aeolian Ridge (Southern Tyrrhenian Sea, Italy). Bull Volcanol. 2013;75(4):710. https://doi.org/10.1007/s00445-013-0710-9.

Ebinger C, Casey M. Continental breakup in magmatic provinces: an Ethiopian example. Geology. 2001;29:527–30.

Ebinger CJ, Yemane T, Harding DJ, Tesfaye S, Kelley S, Rex DC. Rift deflection, migration, and propagation: linkage of the Ethiopian and Eastern rifts. Africa Geol Soc Am Bull. 2000;112:163–76.

Ferguson DJ, Barnie TD, Pyle DM, Oppenheimer C, Yirgu G, Lewi E, Kidane T, Carn S, Hamling I. Recent rift-related volcanism in Afar, Ethiopia. Earth Planet Sci Lett. 2010;292:409–18. https://doi.org/10.1016/j.epsl.2010.02.010.

Georgsson LS, Fridleifsson IB. Geothermal energy in the world and the capacity building activities of the UNU-GTP. In: Presented at short course IX on exploration for geothermal resources. Kenya: UNU-GTP, GDC and KenGen, Kenya; 2013. pp. 1–12

Ghebreab W. Tectonics of the Red Sea region reassessed. Earth Sci Rev. 1998;45:1–44.

Greenfield T, Keir D, Kendall JM, Ayele A. Low-frequency earthquakes beneath Tulu Moye volcano, Ethiopia, reveal fluid pulses from shallow magma chamber. Earth Planet Sci Lett. 2019;526:1–11. https://doi.org/10.1016/j.epsl.2019.115782.

Gunn PJ. Linear transformation of gravity and magnetic fields. Geophys Prospect Sci Res. 1975;23:300–12. https://doi.org/10.1111/j.1365-2478.tb01530.x.

Hardarson BS. The western branch of the East African rift: a review of tectonics, volcanology and geothermal activity. Presented at SDG Short Course II on Exploration and Development of Geothermal Resources, organized by UNU-GTP, GDC and KenGen, at Lake Bogoria and Lake Naivasha, Kenya, 2017; 9–29.

Hayward N, Ebinger C. Variations in a long-axis segmentation of the Afar rift system. Tectonics. 1996;15:244–57.

International Heat Flow Commission (IHFC). Global Heat Flow Map. 2008. http://www.geophysik.rwth-aachen.de/IHFC/heatflow.html. Accessed 13 Nov 2018.

Kasidi S, Nur A. Curie depth isotherm deduced from spectral analysis of magnetic data over Sarti and Environs of North-Eastern Nigeria. Sch J Biotechnol. 2012;1(3):49–56.

Kebede S. Geothermal exploration and development in Ethiopia: country update. In: Short Course IX on exploration for geothermal resources. vol. 15, no. 8; Kenya: UNU-GTP, GDC, and KenGen. 2014. pp. 1–8.

Kebede S. Country update on geothermal exploration and development in Ethiopia. In Proceedings, 6th African Rift geothermal conference. 2016; 1–15.

Kebede S. status of geothermal exploration and development in Ethiopia. Short Course V on Exploration and Development of Geothermal Resources. 2021.

Keir D, Ebinger C, Stuart GW, Daly E, Ayele A. Strain accommodation by magmatism and faulting as rifting proceeds to breakup: seismicity of the northern Ethiopian Rift. J Geophys Res. 2006;111:1–17. https://doi.org/10.1029/2005JB003748.

Keller GR, Harder SH, O'Reilly B, Mickus K, Tadesse K, Maguire PKM, the EAGLE Working Group. A preliminary analysis of crustal structure variations along the Ethiopian Rift, in Yirgu, G., et al., eds., Proceedings of International Conference on the East African Rift System, Addis Ababa, Ethiopia: Ethiopian Geoscience and Mineral Engineering Association. Addis Ababa. 2004; 97–101.

Keranen K, Klemperer SL. Discontinuous and diachronous evolution of the Main Ethiopian Rift: implications for development of continental rifts. Earth Planet Sci Lett. 2008;265:96–111. https://doi.org/10.1016/j.epsl.2007.09.038.

Keranen K, Klemperer S, Gloaguen R, the EAGLE Working Group. Three-dimensional seismic imaging of a protoridge axis in the main Ethiopian rift. Geology. 2004;32:949–52.

Keranen KM, Klemperer SL, Julia J, Lawrence F, Nyblade AA. Low lower crustal velocity across Ethiopia: is the Main Ethiopian Rift a narrow rift in a hot craton? Geochem Geophys Geosyst. 2009;10:1–21. https://doi.org/10.1029/2008GC002293.

Khojamli A, Ardejani FD, Moradzadeh A, Kalate AN, Kahoo RA, Porkhial S. Estimation of curie point depths and heat flow from Ardebil province, Iran, using aeromagnetic data. Arab J Geosci. 2016;9:1–11. https://doi.org/10.1007/s12517-016-2400-3.

Korme T, Acocella V, Abebe B. The role of pre-existing structures in the origin, propagation and architecture of faults in the Main Ethiopian Rift. Gondwana Res. 2004;7(2):467–79.

Kurz T, Gloaguen R, Ebinger C, Casey M, Abebe B. Deformation distribution and type in the Main Ethiopian Rift: a remote sensing study. J Afr Earth Sci. 2007;48:100–14.

Lesur V, Hamoudi M, Choi Y, Dyment J, Erwan T. Building the second version of the World Digital Magnetic Anomaly Map (WDMAM). Earth Planet Space. 2016;68:1–13. https://doi.org/10.1186/s40623-016-0404.

Li CF, Lu Y, Wang J. A global reference model of Curie-point depths based on EMAG2. Sci Rep. 2017;7:1–9. https://doi.org/10.1038/srep45129.

Luo Y, Xue DJ, Wang M. Reduction to the pole at the geomagnetic equator. Chin J Geophys. 2010;53(6):1082–9.

Maguire P, Ebinger C, Stuart G, Mackenzie G, et al. Geophysical project in Ethiopia studies continental breakup. EOS Trans Am Geophys Union. 2003;84(35):337–40. https://doi.org/10.1029/2003EO350002.

Meyer W, Pilger A, Rosler A, Stets J. Tectonic evolution of the northern part of the Main Ethiopian Rift. Afar Depression in Ethiopia. Stuttgart, West Germany, Schweizerhart. 1975; 14: 352–361.

Mickus K, Tadesse K, Keller G, Oluma B. Gravity analysis of the Main Ethiopian Rift. J Afr Earth Sci. 2007;48:59–69. https://doi.org/10.1016/j.jafrearsci.2007.02.008.

Morley CK, Wescott WA, Stone DM, Harper RM, Wigger ST, Karanja FM. Tectonic evolution of the northern Kenyan Rift. J Geol Soc. 1992;149(3):333–48. https://doi.org/10.1144/gsjgs.149.3.0333.

Njeudjang K, Kana JD, Tom A, Abate Essi JM, Djongyang N, Tchinda R. Curie point depth and heat flow deduced from spectral analysis of magnetic data over Adamawa Volcanic Region (Northern Cameroon): geothermal implications. SN Appl Sci. 2020;2:1–16. https://doi.org/10.1007/s42452-020-3099-z.

Oasis Montaj. Geosoft mapping and application system, Inc, Suite 500, Richmond St. West Toronto, ON Canada N5SIV6. 2007.

Odidi GI, Mallam A, Nasir N. Determination of The Curie Point Depth, thermal gradient and heat flow of parts of Central and North-Eastern Nigeria Using Spectral Analysis Technique. 2020.

Okubo Y, Graf JR, Hansen RO, Ogawa K, Tsu H. Curie point depths of the island of Kyushu and surrounding areas, Japan. Geophysics. 1985;53:481–94. https://doi.org/10.1190/1.1441926.

Reed CA, Almadani S, Gao SS, Elsheikh AA, Cherie S, Abdelsalam MG, Liu KH. Receiver function constraints on crustal seismic velocities and partial melting beneath the Red Sea rift and adjacent regions, Afar Depression. J Geophy Res Solid Earth. 2014;119(3):2138–52.

Ross HE, Blakely RJ, Zoback MD. Testing the use of aeromagnetic data for the determination of curie depth in California. Geophysics. 2006;71(5):51-L59.

Saemundsson K. East African Rift System - an overview. Short course III on exploration for geothermal resources, organized by UNU-GTP and KenGen, at Lake Naivasha, Kenya, October 24 - November 17, 2008.

Salem A, Green C, Ravat D, Singh KH, East P, Fairhead JD, Biegert E. Depth to Curie temperature across the central Red Sea from magnetic data using the de-fractal method. Tectonophysics. 2014;624:75–86. https://doi.org/10.1016/j.tecto.2014.04.027.

Schaschke C. A dictionary of chemical engineering. Oxford: Oxford University Press; 2014. https://doi.org/10.1093/acref/9780199651450.001.0001

Shuey RT, Schellinger DK, Tripp AC, Lb A. Curie depth determination from aeromagnetic spectra. Geophys J Int. 1977;50:75–101.

Soengkono S. Airborne magnetic surveys to investigate high temperature geothermal reservoirs. In: Advances in geothermal energy. Croatia: Intech; 2016. p. 113.

Spector A, Grant FS. Statistical models for interpreting aeromagnetic data. Geophysics. 1970;35:293–302.

Tanaka A, Okubo Y, Matsubayashi O. Curie point depth based on spectrum analysis of magnetic anomaly data in East and Southeast Asia. Tectonophysics. 1999;306:461–70.

Tefera M, Chernet T, Haro W, Teshome N, Woldie K. Geological map of Ethiopia 2nd Edition**.** Published by the Regional Mapping Department of the Ethiopian Geological Survey of Ethiopia, Addis Ababa, 1996.

Telford WM, Geldart LP, Sheriff RE. Applied geophysics. 2nd ed. Cambridge: Cambridge University Press; 1990.

Tiberi C, Ebinger C, Ballu V, Stuart G, Oluma B. Inverse models of gravity data from the Red Sea-Aden-East African rifts triple junction zone. Geophys J Int. 2005;163:775–87.

Wolfenden E, Yirgu G, Ebinger C, Ayalew D, Deino A. Evolution of the northern Main Ethiopian rift: birth of a triple junction. Earth Planet Sci Lett. 2004;224:213–28.

Yahya AA, Shimeles F, Muralitharan J. Digital elevation model and satellite gravity anomalies and its correlation with geologic structures at Borena basin, in the Southern Main Ethiopian Rift. Eur J Remote Sens. 2022;55(1):540–50. https://doi.org/10.1080/22797254.2022.2130096.

Yao L. Hartley transform for Reduction to the Pole. Chin J Geophys. 2013;56:572–83. https://doi.org/10.1002/cjg2.20054.

Publisher's Note

Springer Nature remains neutral with regard to jurisdictional claims in published maps and institutional affiliations.